Western Pacific physical and biological controls on atmospheric CO2 concentration over the last 700 kyr

Zheng Tang
First Institute of Oceanography, Ministry of Natural Resources (MNR) https://orcid.org/0000-0003-4908-8982

Zhifang Xiong
First Institute of Oceanography, Ministry of Natural Resources https://orcid.org/0000-0001-9370-0089

Tiegang Li (tgli@fio.org.cn)
First Institute of Oceanography, Ministry of Natural Resources

---

Article

Keywords: glacial terminations, ventilation, stable carbon isotope, CO2 outgassing, western Philippine Sea, Southern Ocean

DOI: https://doi.org/10.21203/rs.3.rs-855845/v1

Abstract

We present new geochemical evidence of changes in the vertical dissolved inorganic carbon (DIC) distribution in the western tropical Pacific over the last 700 kyr, derived from stable carbon isotope ($\delta^{13}C$) signals recorded in epifaunal benthic (*Cibicidoides wuellerstorfi*) and thermocline-dwelling planktonic (*Pulleniatina obliquiloculata*) foraminifera extracted from the Calypso Core MD06-3047. We further analyse the results of a transient numerical experiment of the Last Glacial Maximum (LGM) and the last deglaciation performed with the carbon isotope-enabled earth system model LOVECLIM, to understand the deglacial changes in DIC distribution and verify the proxy-based hypothesis. During glacial periods of the past 700 kyrs, the distinct negative deep water $\delta^{13}C_{DIC}$ values obtained from the benthic foraminifera suggest a carbon increase in the deep ocean, which could have been caused by weakening of deep Southern Ocean (SO) ventilation and enhanced marine biological productivity driven by dust-induced iron fertilization. During glacial terminations, a decrease of thermocline $\delta^{13}C_{DIC}$ associated with an increase in deep water $\delta^{13}C_{DIC}$ indicate a reduced vertical DIC gradient and the net transmission of ^{12}C from the deep waters to the thermocline, caused mainly by the physical process (enhanced SO ventilation). On longer time scales, the largest increase in the Pacific deep carbon reservoir $\delta^{13}C_{DIC}$ during the marine isotope stage (MIS) 12/11 transition coincided with the mid-Brunhes climatic shift, which implies that the extent of oceanic carbon release during this interval was much larger than that during other deglaciations since 700 ka B.P. We infer that this could have been caused by reorganization of the oceanic carbon system. These findings provide new insights into the Pleistocene evolution of the carbon-cycle system in the Pacific Ocean.

Introduction

On glacial-interglacial (G-IG) timescales, gas exchange between the ocean and atmosphere regulates fluctuations in the partial pressure of atmospheric carbon dioxide (pCO_2^{atm})[1], which in turn may amplify the impacts of longer term external climate forcing on Earth's climate[2]. Critically, this exchange involves the lower and upper cells of the global meridional overturning circulation (MOC), which are separated (approximately) by the 27.6 kg m^{-3} density surface[3,4]. The MOC is thought to play a key role in the efficiency of the so-called biological soft-tissue pump (STP) in two ways: first, by facilitating the upward transport of nutrient- and CO_2-rich waters along the density surface, outcropping south of the polar front all the way around Antarctica; and second, by modulating the export of biologically fixed carbon into the ocean interior, where it is remineralized to dissolved inorganic carbon (DIC) and may effectively be isolated from the atmosphere[3,5,6]. Either decreasing the rate of vertical exchange or enhancing export production would raise DIC concentrations in deep waters, thereby lowering pCO_2^{atm}. Increased DIC levels, in turn, enhance deep water corrosivity, possibly dissolving carbonate ($CaCO_3$) minerals and thereby increasing ocean alkalinity, which produces a further CO_2 drawdown[7].

Although the STP efficiency in the Atlantic sector of the Southern Ocean (SO) has received much attention in recent years[5,6,8], the STP efficiency of the Pacific Ocean has received little attention and so remains poorly understood, despite the Pacific Basin dominating the world ocean volumetrically (3× larger than the Atlantic) and deriving its chemical characteristics from the SO. Furthermore, the Pacific Ocean has likely been the potential repository for a large portion of the carbon removed from the atmosphere during glacial periods[9,10,11]. This raises questions concerning the impact of the significant Pacific "organic carbon pump" on pCO_2^{atm}, in particular the balance between biological and physical processes. The Antarctic Intermediate Water (AAIW) originates mainly from the upwelled carbon-rich Pacific Deep Water (PDW)[12]. AAIW forms close to the Sub-Antarctic Front (SAF)[13], with subsequent northward advection into the Pacific subtropical gyre through the low-latitude thermocline. On the other hand, the SO upwelling induced respired carbon outgassing from deep ocean to the atmosphere, may have left an isotopic footprint on the global upper ocean through air-sea exchange[14]. Hence, oceanic and atmospheric teleconnections may be able to propagate geochemical signals to low latitudes[15]. In this context, estimates of the vertical DIC distribution in the low-latitude Pacific obtained through paleo-proxies could possibly provide information on past changes in SO ventilation.

Carbon isotopic gradients derived from benthic and planktonic foraminiferal calcite ($\delta^{13}C_b$ and $\delta^{13}C_p$) can be used to estimate the chemical differences between southern-sourced bottom and upper ocean thermocline waters[16,17]. This approach exploits the recognition that the $\delta^{13}C$ of inorganic carbon dissolved in seawater ($\delta^{13}C_{DIC}$) can be used to trace the nutrient cycling associated with the biological pump in the ocean, because the photosynthetic carbon fixation preferentially removes ^{12}C from the surface layer, leaving the surface ocean enriched in ^{13}C. ^{12}C-enriched carbon exported as organic material is later released to the deeper water column via remineralization, lowering deep ocean $\delta^{13}C_{DIC}$. The balance of biological versus physical (that is, transport and mixing of nutrient- and CO_2-rich water masses) processes therefore controls the magnitude of the vertical $\delta^{13}C_{DIC}$ gradient ($\Delta\delta^{13}C_{DIC}$) between bottom and upper ocean waters. As a result of these competitive processes, nutrients are, in general, negatively correlated with $\delta^{13}C_{DIC}$, and nutrient-rich waters such as the Antarctic Bottom Water (AABW) have relatively low $\delta^{13}C_{DIC}$ values[18].

Here, we present new geochemical evidence of changes in the STP efficiency and vertical DIC distribution over the last 700 kyr, derived from co-registered $\delta^{13}C$ signals recorded in epifaunal benthic (*Cibicidoides wuellerstorfi*) and thermocline-dwelling planktonic (*Pulleniatina obliquiloculata*) foraminifera extracted from the Calypso Core MD06-3047. Altogether, the combination of our carbon isotope results with other proxy data and transient climate simulations performed with the carbon-isotopes enabled Earth system model LOVECLIM[19], help understand G-IG marine carbon cycle changes.

Materials And Methods

Calypso Core MD06-3047 (890 cm long) was retrieved from the Benham Rise of the western Philippine Basin (17°00.44'N, 124°47.93'E; Fig. 1) during the joint Chinese and French cruise MARCO POLO 2/IMAGES XIV in 2006. The core was recovered from a water depth of 2510 m, within PDW. The chemical composition of this water mass is obtained in the Southern Ocean[12]. The bottom water is located beneath the 27.6 kg m^{-3} isopycnal surface, which is the approximate boundary between the upper and lower cells of the global MOC[4]. Here, the subsurface thermocline waters are thought to be strongly influenced by the AAIW[20]. Core MD06-3047 was composed mainly of yellow–brown silty clay and showed no evidence of turbidites or mass redeposition. A detailed description of the geological setting (e.g., topography, ocean current, and wind) in the Philippine Sea was provided by Xu et al[21,22] and Wan et al[23]. The Benham Rise is an oceanic plateau that formed along the Central Basin Ridge at 45–50 Ma[24]. The core site was located about 240 km east of Luzon (Fig. 1). The continental shelves along eastern Luzon are very narrow (< 10 km on average), and the core site was located relatively far from the shelf (~ 230 km), so the effects of sea level variation on fluvial input from Luzon to this site are expected to be negligible. The region of Luzon is dominated by a subtropical East Asian monsoon climate[25].

The core was subsampled at 2-cm intervals and a total of 445 samples were obtained for analysis. The dry weight of these samples was determined and divided by the wet volume of the sample to obtain the dry bulk density. After being dried at 50°C, each sample (5 g dry weight) was treated with 5% H_2O_2 and washed through a 63 μm sieve to recover the foraminiferal tests. Analysis was carried out on planktonic foraminifera samples containing 10–15 specimens of *Pulleniatina obliquiloculata* from the 300–400 μm fraction, and also on the benthic foraminifera *Cibicidoides wuellerstorfi*, using 3–8 specimens picked from the 300–450 μm fraction. To minimize contamination, we were careful not to pick any broken, discoloured, or filled tests for isotopic measurement. The stable isotope ratios of the foraminiferal tests were measured on a GV IsoPrime mass spectrometer at the Key Laboratory of Marine Geology and Environment, Institute of Oceanography, Chinese Academy of Sciences. The analytical precision was better than ± 0.03‰ for $\delta^{13}C$ and ± 0.06‰ for $\delta^{18}O$. Calibration against the Vienna Pee Dee Belemnite (VPDB) was performed using the standard NBS19.

Below, we will compare the signatures from Calypso cores ODP1090 and ANT30/P1-03 (Fig. 1), recovered from the sub-Antarctic zone (SAZ) and Antarctic zone (AZ), respectively, with our record from core MD06-3047, to trace the SO processes in the global carbon cycle.

Model setup and experimental design.

The LGM is a representative period of the glacial patterns in G-IG cycles. In addition, the subsequent Heinrich stadial 1 (HS1), at the beginning of the last deglaciation, is a crucial period to understand as it represents a major phase of atmospheric CO_2 rise and the transition out of the glacial period[11,26]. To better understand the DIC distribution in G-IG cycles and verify the proxy-based hypothesis, we further analyse the results of a transient numerical experiment of the LGM and the last deglaciation performed with the carbon isotope-enabled Earth system model LOVECLIM[26]. LOVECLIM includes an ocean general

circulation model (3° × 3°, 20 vertical levels), a dynamic–thermodynamic sea ice model, a quasigeostrophic atmospheric model (T21, three vertical levels), a land surface scheme, a dynamic global vegetation model and a marine carbon cycle model[27]. The transient simulation starts from the Last Glacial Maximum (LGM) state with weak (11.2 Sv) and shallow NADW, and very weak AABW (5.1 Sv) obtained through 20% weaker SH westerlies and a 0.1 Sv meltwater input into the Southern Ocean[11]. This LGM simulation featured the best model-data agreement in oceanic $\delta^{13}C$ and ventilation age distributions, and include a global mean 0.38 permil lower oceanic $\delta^{13}C$ at the LGM compared to Pre-industrial (PI) interval.

From this LGM state, the model is transiently integrated by varying the orbital parameters[28], and Northern Hemispheric ice-sheet extent, topography and albedo[29]. To simulate a shutdown of NADW during Heinrich stadial 1, meltwater is added to the northern North Atlantic (0.04 Sv until 17.6 ka B.P., 0.07 Sv between 17.6 and 16.2 ka B.P.), while AABW is enhanced by decreasing the buoyancy forcing and strengthening the southern hemispheric westerly windstress.

Results And Discussion

Chronological framework

The chronological framework of core MD06-3047 was obtained by comparing the benthic foraminifera *C. wuellerstorfi* $\delta^{18}O$ curve from this core[30] with that of the LR04 $\delta^{18}O$ stack[31], and also upon consideration of the last appearance datum (LAD) of *G. ruber* (pink). The LAD of *G. ruber* (pink) appeared at a depth of 160 cm, with a known age of 120 ka B.P[32]. Based on this chronology, the period of sediment accumulation spans marine isotope stages (MIS) 1–17, and thus potentially records the paleoceanographic history of the western Pacific (WP) over the last 700 kyr (Fig. 2).

Increased deep carbon storage and STP efficiency in the glacial tropical Pacific

Among genera of benthic foraminifera, the epibenthic dweller *C. wuellerstorfi* seems to record the $\delta^{13}C_{DIC}$ most reliably[33,34]. During glacial intervals, we found distinct negative deep water $\delta^{13}C_{DIC}$ values in benthic foraminifera in our core (Fig. 3C), which is consistent with the benthic $\delta^{13}C$ records from the glacial Pacific deep water (below 2000–2500 m)[35-37] and indicates the sequestration of more respired DIC and nutrients in the deep relative to the interglacials. The very negative glacial deep water $\delta^{13}C$ values are also present in benthic foraminifera from the Atlantic[33,38], Indian Ocean[33,39], and SO (Fig. 3I)[40,41], suggesting that the deep water reservoir stored more carbon in the glacial ocean. This large-scale phenomenon is consistent with the global stacked benthic foraminifera $\delta^{13}C$ record (Fig. 3D)[42]. Here we analyse a numerical experiment of the LGM[11], and hypothesise that it is representative of glacial periods. This LGM simulation displays higher oceanic DIC concentration in the deep ocean compared to PI (Fig. 5A).

Our reconstruction of the $\delta^{13}C_{DIC}$ gradient between the thermocline and deep waters ($\Delta\delta^{13}C_{DIC}$) shows that the largest difference coincides with full glacial conditions, indicating a more efficient STP in the western tropical Pacific, when pCO_2^{atm} was at its lowest (Fig. 3E, N), which is consistent with recent STP records from the SO reported in recent studies[5,6,8]. Processes that impact the whole-ocean $\delta^{13}C$, such as the transport of terrestrial organic material with relatively low levels of $\delta^{13}C$ to the oceans during glacial periods, are unlikely to result in $\delta^{13}C_{DIC}$ gradient variation as they impact the entire water column equally. During glacial intervals, relatively high Antarctic sea ice cover (Fig. 3L)[43] and the northward movement and/or weakening of the Southern Hemisphere (SH) westerlies (Fig. 3M)[44] are believed to have the potential to significantly attenuate the ventilation of the ocean's interior[3,7,45], which is in line with the isolated old glacial water masses identified in the North and South Pacific, as well as in the South Atlantic[11,46-48]. The higher glacial export production in the WP, as recorded by variations in production of total organic carbon and mass accumulate rate (TOC*MAR; Fig. 3F)[49], could also reinforce the STP in the tropical Pacific. The observed close correlation between variations in dust supply and export production (Fig. 3F, G) indicates a dust-driven strengthening of the biological organic pump in the WP[49]. The glacial enhanced iron-bearing dust inputs to the WP caused by the strengthened winter monsoon winds/westerlies and increased aridity in central Asia (Fig. 3G)[22,23,49], might stimulate nutrient utilization and phytoplankton growth, thus leading to high biological productivity (Fig. 3F)[49,50]. Moreover, an increased WP nutrient drawdown and carbon transfer to the deep ocean stimulates an alkalinity feedback through the dissolution of carbonate in the abyss[51]. From the above, the weakening of the deep SO ventilation and the enhanced organic biological productivity by dust-induced iron fertilization via the synergy of both physical and biological processes led to a more efficient STP in the glacial tropical Pacific, hence contributing to the pCO_2^{atm} drawdown.

Role of SO ventilation in the vertical DIC distribution of the tropical Pacific

Pulleniatina obliquiloculata is the subsurface-dwelling planktonic foraminifera that is most abundant in middle to upper thermocline depths[52,53]. The significant carbon isotope minimum events (CIMEs) that occurred during glacial terminations (Fig. 3B) resemble planktonic $\delta^{13}C$ profiles that are found in the equatorial Pacific[54-56] as well as in the high- and mid-latitude SO[8,41]. The CIMEs could reflect the collapse of deep ocean stratification, enhanced upwelling in the SO of low-$\delta^{13}C_{DIC}$ and CO_2-laden aged deep waters[45,57]. The negative-$\delta^{13}C$ signal might be transmitted to thermocline of low-latitude ocean via ocean circulation (formation and advection of AAIW)[54], and the air-sea equilibration (strong outgassing in the SO and the ocean-atmosphere equilibrium thermodynamic exchange)[14,57].

The pronounced decreases in the ^{14}C ventilation age in the South Pacific[47,58] and in the $\delta^{13}C$ of atmospheric CO_2[59] during glacial terminations provide further evidence of enhanced ventilation of old and low-$\delta^{13}C_{DIC}$ deep Southern water mass to the surface and subsequent CO_2 outgassing. The

prominence of CIMEs in our record updates evidence that the $\delta^{13}C$ record of *P. obliquiloculata* reliably traces the enhanced SO ventilation.

During glacial terminations, the significant CIMEs reveal the migration of DIC and nutrients from the deep carbon pool to the low-latitude thermocline by intense SO ventilation and subsequently oceanic and atmospheric teleconnections[14,45,54,57]. As a result of the ventilation-caused "DIC transmission", we hypothesize that not only the ocean upper layer and atmospheric CO_2 could receive the low-$\delta^{13}C_{DIC}$ signal during deglaciations (Fig. 4C)[59], but the southern-sourced deep carbon reservoir would receive the rising $\delta^{13}C_{DIC}$ signal. The most compelling support for our hypothesis comes from the antiphase variation of the thermocline and deep water $\delta^{13}C_{DIC}$ recorded in core MD06-3047 during each termination (Fig. 4C, D). If our hypothesis is correct, more widely distributed records of deep-ocean benthic $\delta^{13}C$ would capture the release of the deep low-$\delta^{13}C_{DIC}$ carbon reservoir. During Termination I–VII, the sub-Antarctic Zone (SAZ) deep water $\delta^{13}C_{DIC}$ from ODP 1090 (Fig. 4B)[40] and global stacked benthic foraminifera $\delta^{13}C$ increased as expected (Fig. 4E), possibly suggesting a transfer of a low-$\delta^{13}C_{DIC}$ signal from the depth to the surface. It is worth noting that the planktonic and benthic $\delta^{13}C$ did not always vary in antiphase in ODP 1090 (i.e., T-I and T-IV in Fig. 4A, B). In addition, their inverse trends began earlier and lasted longer (Fig. 3H, I). We suggest that the relatively reduced distance between ODP 1090 and the SO upwelling outcropping south of the Polar Front made the deep and upper layers of the core more sensitive and direct to the enhanced SO ventilation.

To further understand the ventilation-driven vertical DIC antiphase and verify our proxy-based hypothesis, we analyse the results of a transient numerical modelling experiment performed LOVECLIM[26]. Because at the beginning of the last deglaciation, HS1 represents a major phase of atmospheric CO_2 rise and the transition out of the glacial periods, we chose HS1 in the last glacial-interglacial transition as a representative of the glacial terminations in G-IG cycles. Enhanced upwelling of DIC-rich CDW at the surface of the SO leads to a DIC increase in the upper 500m depth. The associated stronger AABW, and AAIW transport, lead to a DIC decrease in the SO and in the Pacific Ocean below ~1000m depth (Fig. 5B). Due to oceanic and atmospheric teleconnections, North Pacific Intermediate Waters (NPIW) also strengthen and ventilate during HS1[60]. This leads to a DIC decrease at intermediate depth of the North Pacific, not far above our core-site depth (Fig. 5B), and thus might potentially contributes to the DIC decrease in our record (Fig. 4D). These changes in oceanic circulation leads to a $\delta^{13}C$ increase in the intermediate and deep Pacific, while $\delta^{13}C$ decreases at the surface of the ocean (Fig. 5C). This is consistent with our proxy record of $\delta^{13}C_{DIC}$ (Fig. 4C, D).

The SO ventilation has the potential to drive the antiphase variation of the vertical DIC distribution during glacial terminations. Meltwater input in the northern Atlantic/Arctic, due to Northern Hemisphere ice sheet retreat induced a cessation of the Atlantic MOC[61-63]. This process, in conjunction with Antarctic local orbital forcing[44,64], might have triggered the decline in sea ice[43,65](Fig. 4G) and southward movement/enhancement of the SH westerlies[45,66-68](Fig. 4H). Stronger westerlies would have enhanced

the SO upwelling[4,45]. This would have led to CO_2 outgassing and a decrease in $\delta^{13}C$ of atmospheric CO_2[26,59](Fig. 4J). This is also consistent with enhanced diatom productivity in the SO[45,69,70] (Fig. 4I). In addition, through oceanic and atmospheric teleconnections, cessation of the Atlantic MOC enhances the formation of NPIW, thus ventilating the intermediate North Pacific[26,60,71]. This might lead to a DIC decrease at intermediate and deep depth of the North Pacific, in agreement with the Ice-rafted debris (IRD) record in northern Atlantic[72](Fig. 4F) and our paleo and model results (Fig. 4D, Fig. 5B). So we suggest the NPIW enhancement might might potentially contributes to the DIC decrease at intermediate depth of the North Pacific.

The cause of STP efficiency collapse during glacial terminations

The graphical consistency of STP efficiency in the tropical Pacific and pCO_2^{atm} may point to the role of the low-latitude biological pump in changing the global climate (Fig. 3E, N), especially during glacial terminations. In glacial–interglacial transitions, the STP efficiency collapses corresponded to significant increases in pCO_2^{atm}. However, it remains to be determined whether the observed decrease in “organic carbon pump” efficiency resulted primarily from decreases in export productivity, or increases in ocean “ventilation”. We address this question by reference to our export productivity and the $\delta^{13}C_{DIC}$ of the thermocline and deep waters. The export productivity, as recorded by the variation in TOC*MAR (Fig. 3F) reduced significantly during Termination I, III, IV, and V, but the changes during Termination II and VI were too small to have altered the STP. Increases in $\delta^{13}C_b$ and reductions in $\delta^{13}C_p$ during glacial terminations indicate ^{12}C transmission through ventilation from the deep to the upper layer. However, photosynthetic carbon fixation preferentially removes ^{12}C from the surface-layer DIC to the deeper water column. This process could explain the net transmission of ^{12}C from deep to thermocline only be the enhanced ventilation, disagree with the proposition that a more poorly ventilated deep Pacific (relative to today) did not or could not exist[73,74]. During glacial terminations, the physical process (enhanced SO ventilation) was far more effective than the biological process (export productivity) in driving the STP efficiency collapse (Fig. 3E).

Coordination of physical and biological controls on pCO_2^{atm} changes

Our findings reveal insights into the coordination between physical and biological controls on pCO_2^{atm} changes over glacial cycles in the WP, and these are consistent with recently published sedimentary redox records from the AZ and SAZ[5,6]. This suggests that the coordination is not only confined to the high- and mid-latitudes in the SO, but also occurs in the low latitudes in the WP, and is related to changes in the interhemispheric oceanic and atmospheric circulations[8]. During glacial periods, the intense stratification of the ocean interior induced by extensive Antarctic sea ice cover[43] (Fig. 3 and 7A) and northward movement and/or weakening of the SH westerlies[44](Figs 3 and 7A), combined with the high biological productivity caused by strengthened winter monsoon winds and increased aridity in central Asia, induced elevated iron-bearing dust inputs into the WP[22,23,49](Figs 3 and 7A), which led to the

continuous "recharge" of the abyssal carbon reservoir. In this light, it may seem remarkable that changes in dust fluxes and deep ventilation were coordinated, reinforcing their synergistic impacts on the STP.

We suggest that there was a mechanistic link between the coordinated physical and biological processes, which involved ventilation and Fe supply, in the high and low latitudes. Owing to this coupling of oceanic and atmospheric circulations, enhanced deglacial deep SO ventilation generally co-occurred with the southward migration of the SH westerlies. The subsequent warming of the atmosphere would have weakened the winter monsoon, which would have led to lower dust inputs to the WP[23,49], causing limited nutrient utilization and facilitating CO_2 outgassing (Fig. 7B). As such, the Fe fertilization processes may be viewed as a positive feedback process in response to initial forcing related to changes in the interhemispheric ocean–atmosphere system[8]. Thus, shifts in atmospheric circulation, coupled with changes in the MOC, would have caused the intensity of Fe limitation and deep convection to co-vary over glacial cycles. These large-scale coupled processes (i.e., coordinating the input flux of carbon to the deep sea and deep ventilation-caused carbon leakage in both high and low latitudes) could together modify the whole-ocean STP efficiency and atmospheric CO_2 levels. Further use of paleoclimate modelling to precisely quantity the contributions of biological/physical processes and high/low latitudes to STP efficiency will be required if we are to fully understand the natural variability of atmospheric CO_2.

Largest-amplitude DIC changes in deep waters at the MIS 12/11 transition

The most significant feature of the MD06-3047 deep-water $\delta^{13}C_{DIC}$ record may be the increase of ~0.97‰ (from −0.50‰ to 0.47‰) between late MIS 12 (ca. 438 ka B.P.) and mid-MIS 11 (ca. 405 ka B.P.), which represents the largest change of this type during the past 700 kyr (Fig. 3C). This peculiar interval also coincided with the largest change in the marine $\delta^{18}O$ record of the last 5 Myr[31], and has been described as a major step change in global climate conditions[75].

This largest increase in the Pacific deep carbon reservoir $\delta^{13}C_{DIC}$ was generated by the most enhanced ventilation-caused “DIC” transmission", which led to a transfer of carbon from the deep ocean to the atmosphere[45,76]. Meanwhile, the breakdown of oceanic stratification would raise the deep-water carbonate ion concentration ($[CO_3^{2-}]$) and $CaCO_3$ preservation[51,77]. In a recent study, the reconstructed deep water $[CO_3^{2-}]$ in this water column (from the same sediment core MD06-3047B) reached its maximum at the MIS12/11 termination[78](Fig. 6B). Furthermore, the “Pacific-style” $CaCO_3$ content records[79](Fig. 6C) also show their preservation maxima at the MIS 12/11 boundary. The extremely high values of these records during the MIS 12/11 transition imply that the extent of oceanic carbon release during this interval was much larger than during other deglaciations since 700 ka B.P.

Conclusions

Our reconstruction of vertical DIC distribution for the western tropical Pacific since 700 ka B.P. using a combination of carbon isotope results and climate simulations generated the following conclusions.

(1) The distinct negative deep water $\delta^{13}C_{DIC}$ values obtained from the benthic foraminifera suggest that the deep reservoir stored more carbon in the glacial ocean over the past 700 kyr. The more efficient STP in the glacial tropical Pacific and the drawdown of pCO_2^{atm}, possibly caused by the weakening of the deep SO ventilation and the enhanced organic biological productivity driven by dust-induced iron fertilization, via the coordination of physical and biological controls.

(2) The antiphase variation of the thermocline and deep water $\delta^{13}C_{DIC}$ in our record during each termination is consistent with the deglacial modelling result, suggesting that SO ventilation has the potential to drive the inverse variation of the vertical DIC distribution during glacial terminations.

(3) The increase in $\delta^{13}Cb$ and decrease in $\delta^{13}Cp$ during glacial terminations indicates the net transmission of ^{12}C from the deep waters to the thermocline, and this suggests that the physical process (enhanced SO ventilation) was far more effective than the biological process (export productivity), thus driving the STP efficiency collapse and significant pCO_2^{atm} increase.

(4) This largest increase in the Pacific deep carbon reservoir $\delta^{13}C_{DIC}$ during the MIS 12/11 transition coincided with the mid-Brunhes climatic shift, which implies that the extent of oceanic carbon release during this interval was much larger than that during other deglaciations since 700 ka B.P. We infer that this could have been caused by reorganization of the oceanic carbon system.

Declarations

Acknowledgments

We thank the MARCO POLO 2/IMAGES XIV cruise members for retrieving the sediments, and are grateful to authors who have provided us with data on request or via online repositories. We sincerely thank Associate Professor Laurie Menviel from Climate Change Research Centre, University of New South Wales for her kind model outputs, figure drawings and manuscript revision. This work was supported by the National Natural Science Foundation of China (grant numbers 41830539, 41976080, 91858106, and 41406220), the Basic Scientific Fund for National Public Research Institutes of China (grant numbers 2019Q09, 2019S04 and 2017Y07), the Taishan Scholars Project Funding (grant numbers ts20190963), Evaluation and Effect of Paleoclimatic Evolution (grant number GASI-04-QYQH-04), and Impact and Response of Antarctic Seas to Climate Change (IRASCC2020-2022-01-03-02 and 02-03).

Author contributions

Zheng Tang carried out the foraminifera picking and stable isotope measurements, and together with Zhifang Xiong and Tiegang Li analyzed the data. Zheng Tang contributed the combination of data and model. Tiegang Li helped shape the initial concept and contribute to data interpretation. Zheng Tang wrote the manuscript with contribution from Zhifang Xiong. All the co-authors contributed to the interpretation of the results and provided inputs to the final version.

Competing interests

The authors declare no competing interests.

References

1. Petit, J. R. *et al.* Climate and atmospheric history of the past 420,000 years from the Vostok ice core, Antarctica. *Nature* **399**, 429-436, doi:10.1038/20859 (1999).

2. Sigman, D. M. & Boyle, E. A. Glacial/interglacial variations in atmospheric carbon dioxide. *Nature* **407**, 859-869 (2000).

3. Toggweiler, J. R., Russell, J. L. & Carson, S. R. Midlatitude westerlies, atmospheric CO2, and climate change during the ice ages. *Paleoceanography* **21** (2006).

4. Marshall, J. & Speer, K. Closure of the meridional overturning circulation through Southern Ocean upwelling. *Nature Geoscience* (2012).

5. Jaccard, S. L., Galbraith, E. D., Martínez-García, A. & Anderson, R. F. Covariation of deep Southern Ocean oxygenation and atmospheric CO_2 through the last ice age. *Nature* **530**, 207-210, doi:10.1038/nature16514 (2016).

6. Gottschalk, J. *et al.* Biological and physical controls in the Southern Ocean on past millennial-scale atmospheric CO_2 changes. *Nat Commun* **7**, doi:10.1038/ncomms11539 (2016).

7. Sigman, D. M., Hain, M. P. & Haug, G. H. The polar ocean and glacial cycles in atmospheric CO2 concentration. *Nature* **466**, 47-55 (2010).

8. Ziegler, M., Diz, P., Hall, I. R. & Zahn, R. Millennial-scale changes in atmospheric CO2 levels linked to the Southern Ocean carbon isotope gradient and dust flux. *Nature Geoscience* **6**, 457-461 (2013).

9. Jaccard, S. L. *et al.* Subarctic Pacific evidence for a glacial deepening of the oceanic respired carbon pool. *Earth and Planetary Science Letters* **277**, 156-165 (2009).

10. Bradtmiller, L. I., Anderson, R. F., Sachs, J. P. & Fleisher, M. Q. A deeper respired carbon pool in the glacial equatorial Pacific Ocean. *Earth and Planetary Science Letters* **299**, 417-425 (2010).

11. Menviel, L. *et al.* Poorly ventilated deep ocean at the Last Glacial Maximum inferred from carbon isotopes: A data-model comparison study. *Paleoceanography* **32**, 2-17, doi:https://doi.org/10.1002/2016PA003024 (2017).

12. Talley, L. D. Closure of the global overturning circulation through the Indian, Pacific, and Southern Oceans: Schematics and transports. *Oceanography* **26**, 80-97 (2013).

13. Talley, L. D. in Mechanisms of Global Climate Change at Millennial Time Scales. 1-22 (1999).

Duplessy, J.-C. *et al.* 13C record of benthic foraminifera in the last interglacial ocean: implications for the carbon cycle and the global deep water circulation. *Quaternary Research* **21**, 225-243 (1984).

14. Lynch-Stieglitz, J., Valley, S. G. & Schmidt, M. W. Temperature-dependent ocean–atmosphere equilibration of carbon isotopes in surface and intermediate waters over the deglaciation. *Earth and Planetary Science Letters* **506**, 466-475 (2019).

15. Sarmiento, J., Gruber, N., Brzezinski, M. & Dunne, J. High-latitude controls of thermocline nutrients and low latitude biological productivity. *Nature* **427**, 56-60 (2004).

16. Charles, C. D. *et al.* Millennial scale evolution of the Southern Ocean chemical divide. *Quaternary Science Reviews* **29**, 399-409 (2010).

17. Curry, W. B., Duplessy, J. C., Labeyrie, L. D. & Shackleton, N. J. Changes in the distribution of $\delta^{13}C$ of deep water ΣCO_2 between the Last Glaciation and the Holocene. *Paleoceanography & Paleoclimatology* **3**, 317-341 (1988).

18. Kroopnick, P. The distribution of 13C of ΣCO2 in the world oceans. *Deep Sea Research Part A. Oceanographic Research Papers* **32**, 57-84 (1985).

19. Menviel, L., Mouchet, A., Meissner, K. J., Joos, F. & England, M. H. Impact of oceanic circulation changes on atmospheric δ13CO2. *Global Biogeochemical Cycles* **29**, 1944-1961, doi:https://doi.org/10.1002/2015GB005207 (2015).

20. Tsuchiya, M., Lukas, R., Fine, R. A., Firing, E. & Lindstrom, E. Source waters of the Pacific equatorial undercurrent. *Progress in Oceanography* **23**, 101-147 (1989).

21. Xu, Z., Li, A., Jiang, F. & Xu, F. Geochemical character and material source of sediments in the eastern Philippine Sea. *Chinese Science Bulletin* **53**, 923-931 (2008).

22. Xu, Z. *et al.* Evolution of East Asian monsoon: Clay mineral evidence in the western Philippine Sea over the past 700kyr. *Journal of Asian Earth Sciences* **60**, 188-196 (2012).

23. Wan, S. *et al.* History of Asian eolian input to the West Philippine Sea over the last one million years. *Palaeogeography, Palaeoclimatology, Palaeoecology* **326-328**, 152-159, doi:10.1016/j.palaeo.2012.02.015 (2012).

24. Hilde, T. W. & Chao-Shing, L. Origin and evolution of the West Philippine Basin: a new interpretation. *Tectonophysics* **102**, 85-104 (1984).

25. Liu, Z., Zhao, Y., Colin, C., Siringan, F. P. & Wu, Q. Chemical weathering in Luzon, Philippines from clay mineralogy and major-element geochemistry of river sediments. *Applied Geochemistry* **24**, 2195-2205

(2009).

26. Menviel, L. et al. Southern Hemisphere westerlies as a driver of the early deglacial atmospheric CO2 rise. Nature Communications 9, 2503, doi:10.1038/s41467-018-04876-4 (2018).

27. Goosse, H. *et al.* Description of the Earth system model of intermediate complexity LOVECLIM version 1.2. *Geoscientific Model Development* **3**, 603-633 (2010).

28. Berger, A. Long-term variations of daily insolation and Quaternary climatic changes. *Journal of Atmospheric Sciences* **35**, 2362-2367 (1978).

29. Abe-Ouchi, A., Segawa, T. & Saito, F. Climatic conditions for modelling the Northern Hemisphere ice sheets throughout the ice age cycle. *Climate of the Past* **3**, 423-438 (2007).

30. Tang, Z., Li, T., Chang, F., Nan, Q. & Li, Q. Paleoproductivity evolution in the West Philippine Sea during the last 700 ka. *Chinese Journal of Oceanology and Limnology* **31**, 435-444 (2013).

31. Lisiecki, L. E. & Raymo, M. E. A Pliocene-Pleistocene stack of 57 globally distributed benthic $\delta^{18}O$ records. *Paleoceanography* **20**, PA1003, doi:10.1029/2004pa001071 (2005).

32. Thompson, P. R., Be, A. W. H., Duplessy, J.-C. & Shackleton, N. J. Disappearance of pink-pigmented Globigerinoides ruber at 120,000 yr BP in the Indian and Pacific Oceans. *Nature* **280**, 554-558 (1979).

33. Duplessy, J. *et al.* Deepwater source variations during the last climatic cycle and their impact on the global deepwater circulation. *Paleoceanography* **3**, 343-360 (1988).

34. Graham, D. W., Corliss, B. H., Bender, M. L. & Keigwin Jr, L. D. Carbon and oxygen isotopic disequilibria of recent deep-sea benthic foraminifera. *Marine micropaleontology* **6**, 483-497 (1981).

35. Herguera, J. C. Deep-sea benthic foraminifera and biogenic opal: glacial to postglacial productivity changes in the western equatorial Pacific. *Marine Micropaleontology* **19**, 79-98 (1992).

36. Keigwin, L. D. Glacial-age hydrography of the far northwest Pacific Ocean. *Paleoceanography* **13**, 323-339 (1998).

37. Matsumoto, K., Oba, T., Lynch-Stieglitz, J. & Yamamoto, H. Interior hydrography and circulation of the glacial Pacific Ocean. *Quaternary Science Reviews* **21**, 1693-1704 (2002).

38. Curry, W. B. & Oppo, D. W. Glacial water mass geometry and the distribution of $\delta^{13}C$ of ΣCO2 in the western Atlantic Ocean. *Paleoceanography* **20** (2005).

39. McCorkle, D. C., Heggie, D. T. & Veeh, H. H. Glacial and Holocene stable isotope distributions in the southeastern Indian Ocean. *Paleoceanography* **13**, 20-34 (1998).

40. Hodell, D. A., Venz, K. A., Charles, C. D. & Ninnemann, U. S. Pleistocene vertical carbon isotope and carbonate gradients in the South Atlantic sector of the Southern Ocean. *Geochemistry, Geophysics, Geosystems* **4**, 1-19 (2003).

41. Ninnemann, U. S. & Charles, C. D. Changes in the mode of Southern Ocean circulation over the last glacial cycle revealed by foraminiferal stable isotopic variability. *Earth and Planetary Science Letters* **201**, 383-396 (2002).

42. Hoogakker, B. A. A., Rohling, E. J., Palmer, M. R., Tyrrell, T. & Rothwell, R. G. Underlying causes for long-term global ocean δ13C fluctuations over the last 1.20 Myr. *Earth and Planetary Science Letters* **248**, 15-29, doi:http://dx.doi.org/10.1016/j.epsl.2006.05.007 (2006).

43. Wolff, E. W. *et al.* Southern Ocean sea-ice extent, productivity and iron flux over the past eight glacial cycles. *Nature* **440**, 491-496, doi:http://www.nature.com/nature/journal/v440/n7083 (2006).

44. WAIS Divide Project Members. Onset of deglacial warming in West Antarctica driven by local orbital forcing. *Nature* **500**, 440-444 (2013).

45. Anderson, R. *et al.* Wind-driven upwelling in the Southern Ocean and the deglacial rise in atmospheric CO_2. *Science* **323**, 1443-1448 (2009).

46. Skinner, L. C., Fallon, S., Waelbroeck, C., Michel, E. & Barker, S. Ventilation of the deep Southern Ocean and deglacial CO2 rise. *Science* **328**, 1147-1151 (2010).

47. Skinner, L. *et al.* Reduced ventilation and enhanced magnitude of the deep Pacific carbon pool during the last glacial period. *Earth and Planetary Science Letters* **411**, 45-52, doi:http://dx.doi.org/10.1016/j.epsl.2014.11.024 (2015).

48. Sarnthein, M., Schneider, B. & Grootes, P. M. Peak glacial 14C ventilation ages suggest major draw-down of carbon into the abyssal ocean. *Climate of the Past* **9**, 2595-2614 (2013).

49. Xu, Z. *et al.* Quantitative estimates of Asian dust input to the western Philippine Sea in the mid-late Quaternary and its potential significance for paleoenvironment. *Geochemistry, Geophysics, Geosystems* **16**, 3182-3196 (2015).

50. Xiong, Z. et al. Potential role of giant marine diatoms in sequestration of atmospheric CO2 during the Last Glacial Maximum: δ13C evidence from laminated Ethmodiscus rex mats in tropical West Pacific. Global and Planetary Change 108, 1-14 (2013).

51. Boyle, E. A. The role of vertical chemical fractionation in controlling late Quaternary atmospheric carbon dioxide. *Journal of Geophysical Research: Oceans* **93**, 15701-15714, doi:https://doi.org/10.1029/JC093iC12p15701 (1988).

52. Curry, W. B. & Lohmann, G. Carbon isotopic changes in benthic foraminifera from the western South Atlantic: Reconstruction of glacial abyssal circulation patterns. *Quaternary Research* **18**, 218-235 (1982).

53. Faul, K. L., Ravelo, A. C. & Delaney, M. Reconstructions of upwelling, productivity, and photic zone depth in the eastern equatorial Pacific Ocean using planktonic foraminiferal stable isotopes and abundances. *The Journal of Foraminiferal Research* **30**, 110-125 (2000).

54. Spero, H. J. & Lea, D. W. The Cause of Carbon Isotope Minimum Events on Glacial Terminations. *Science* **296**, 522-525, doi:10.1126/science.1069401 (2002).

55. Pena, L. D., Cacho, I., Ferretti, P. & Hall, M. A. El Niño-Southern Oscillation:like variability during glacial terminations and interlatitudinal teleconnections. *Paleoceanography* **23**, PA3101, doi:10.1029/2008pa001620 (2008).

56. Chen, S. *et al.* Response of the northwestern Pacific upper water $\delta^{13}C$ to the last deglacial ventilation of the deep Southern Ocean. *Chinese Science Bulletin* **56**, 2628-2634, doi:10.1007/s11434-011-4590-0 (2011).

57. Shao, J. *et al.* The Atmospheric Bridge Communicated the δ 13 C Decline during the Last Deglaciation to the Global Upper Ocean. *Climate of the Past Discussions*, 1-28 (2020).

58. Siani, G. *et al.* Carbon isotope records reveal precise timing of enhanced Southern Ocean upwelling during the last deglaciation. *Nature communications* **4** (2013).

59. Schmitt, J. *et al.* Carbon isotope constraints on the deglacial CO2 rise from ice cores. *Science* **336**, 711-714 (2012).

60. Okazaki, Y. *et al.* Deepwater formation in the North Pacific during the last glacial termination. *Science* **329**, 200-204 (2010).

61. McManus, J. F., Francois, R., Gherardi, J. M., Keigwin, L. D. & Brown-Leger, S. Collapse and rapid resumption of Atlantic meridional circulation linked to deglacial climate changes. *Nature* **428**, 834-837, doi:http://www.nature.com/nature/journal/v428/n6985/suppinfo/nature02494_S1.html (2004).

62. Zhang, X., Lohmann, G., Knorr, G. & Xu, X. Different ocean states and transient characteristics in Last Glacial Maximum simulations and implications for deglaciation. *Clim. Past* **9**, 2319-2333, doi:10.5194/cp-9-2319-2013 (2013).

63. Ng, H. C. et al. Coherent deglacial changes in western Atlantic Ocean circulation. *Nature Communications* **9**, 2947, doi:10.1038/s41467-018-05312-3 (2018).

64. Laepple, T., Werner, M. & Lohmann, G. Synchronicity of Antarctic temperatures and local solar insolation on orbital timescales. *Nature* **471**, 91-94 (2011).

65. Stephens, B. B. & Keeling, R. F. The influence of Antarctic sea ice on glacial-interglacial CO2 variations. *Nature* **404**, 171-174 (2000).

66. Law, M., Matear, J. & Francey, J, Comment on" Saturation of the Southern Ocean CO_2 Sink Due to Recent Climate Change" *Science* **319,** 570-570(2008).

67. Toggweiler, J. R. & Russell, J. Ocean circulation in a warming climate. *Nature* **451**, 286-288 (2008).

68. Govin, A. *et al.* Evidence for northward expansion of Antarctic Bottom Water mass in the Southern Ocean during the last glacial inception. *Paleoceanography* **24** (2009).

69. Tang, Z. *et al.* Deglacial biogenic opal peaks revealing enhanced Southern Ocean upwelling during the last 513 ka. *Quaternary International* **425**, 445-452, doi:https://doi.org/10.1016/j.quaint.2016.09.020 (2016).

70. Meckler, A. *et al.* Deglacial pulses of deep-ocean silicate into the subtropical North Atlantic Ocean. *Nature* **495**, 495-498 (2013).

71. Rae, J. W. B. *et al.* Deep water formation in the North Pacific and deglacial CO2 rise. *Paleoceanography* **29**, 645-667, doi:https://doi.org/10.1002/2013PA002570 (2014).

72. Barker, S. *et al.* Icebergs not the trigger for North Atlantic cold events. *Nature* **520**, 333-336, doi:10.1038/nature14330 (2015)

73. Broecker, W., Clark, E. & Barker, S. Near constancy of the Pacific Ocean surface to mid-depth radiocarbon-age difference over the last 20 kyr. *Earth and Planetary Science Letters* **274**, 322-326 (2008).

74. Hain, M. P., Sigman, D. M. & Haug, G. H. Shortcomings of the isolated abyssal reservoir model for deglacial radiocarbon changes in the mid-depth Indo-Pacific Ocean. *Geophysical Research Letters* **38** (2011).

75. Droxler, A. W., Alley, R. B., Howard, W. R., Poore, R. Z., & Burckle, L. H. *Unique and exceptionally long interglacial marine isotope stage 11: Window into Earth warm future climate. Earth's Climate and Orbital Eccentricity: The Marine Isotope Stage 11 Question.*, 1-14 (2003).

76. Martínez-Botí, M. A. *et al.* Boron isotope evidence for oceanic carbon dioxide leakage during the last deglaciation. *Nature* **518**, 219-222, doi:10.1038/nature14155 (2015).

77. Boyle, E. A. Vertical oceanic nutrient fractionation and glacial/interglacial CO_2 cycles. *Nature* **331**, 55, doi:10.1038/331055a0 (1988b).

78. Qin, B., Li, T., Xiong, Z., Algeo, T. & Jia, Q. Deep-Water Carbonate Ion Concentrations in the Western Tropical Pacific Since the Mid-Pleistocene: A Major Perturbation During the Mid-Brunhes. *Journal of Geophysical Research: Oceans* **123**, 6876-6892 (2018).

79. Hodell, D. A., Charles, C. D. & Sierro, F. J. Late Pleistocene evolution of the ocean's carbonate system. *Earth and Planetary Science Letters* **192**, 109, doi:10.1016/s0012-821x(01)00430-7 (2001).

80. Key, R. M. *et al.* A global ocean carbon climatology: Results from Global Data Analysis Project (GLODAP). *Global biogeochemical cycles* **18** (2004).

81. Schlitzer, R. Ocean Data View, https://odv.awi.de. (2020).

82. Martínez-Garcia, A. et al. Southern Ocean dust–climate coupling over the past four million years. Nature 476, 312-315 (2011).

83. Bazin, L. *et al.* An optimized multi-proxy, multi-site Antarctic ice and gas orbital chronology (AICC2012): 120–800 ka. *Climate of the Past* **9**, 1715-1731 (2013).

84. Siegenthaler, U. et al. Stable Carbon Cycle : Climate Relationship During the Late Pleistocene. *Science* **310**, 1313-1317, doi:10.1126/science.1120130 (2005).

Figures

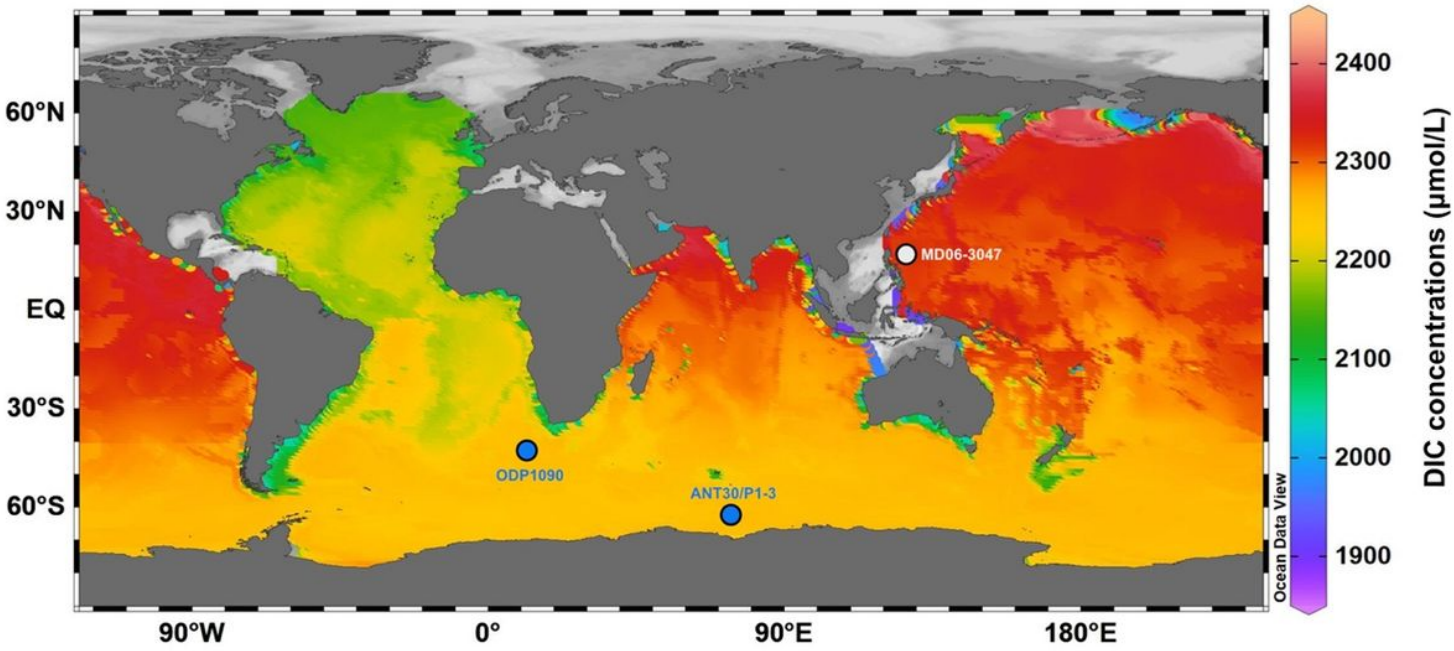

Figure 1

Map showing the locations of Calypso cores investigated in this study and modern ocean DIC concentration (shaded) in bottom waters80. Core MD06-3047 (white circle) is located in the West Philippine Sea, and Cores ODP 1090 and ANT30/P1-03 (blue circles) in the SO. The map was created using the Ocean Data View software81.

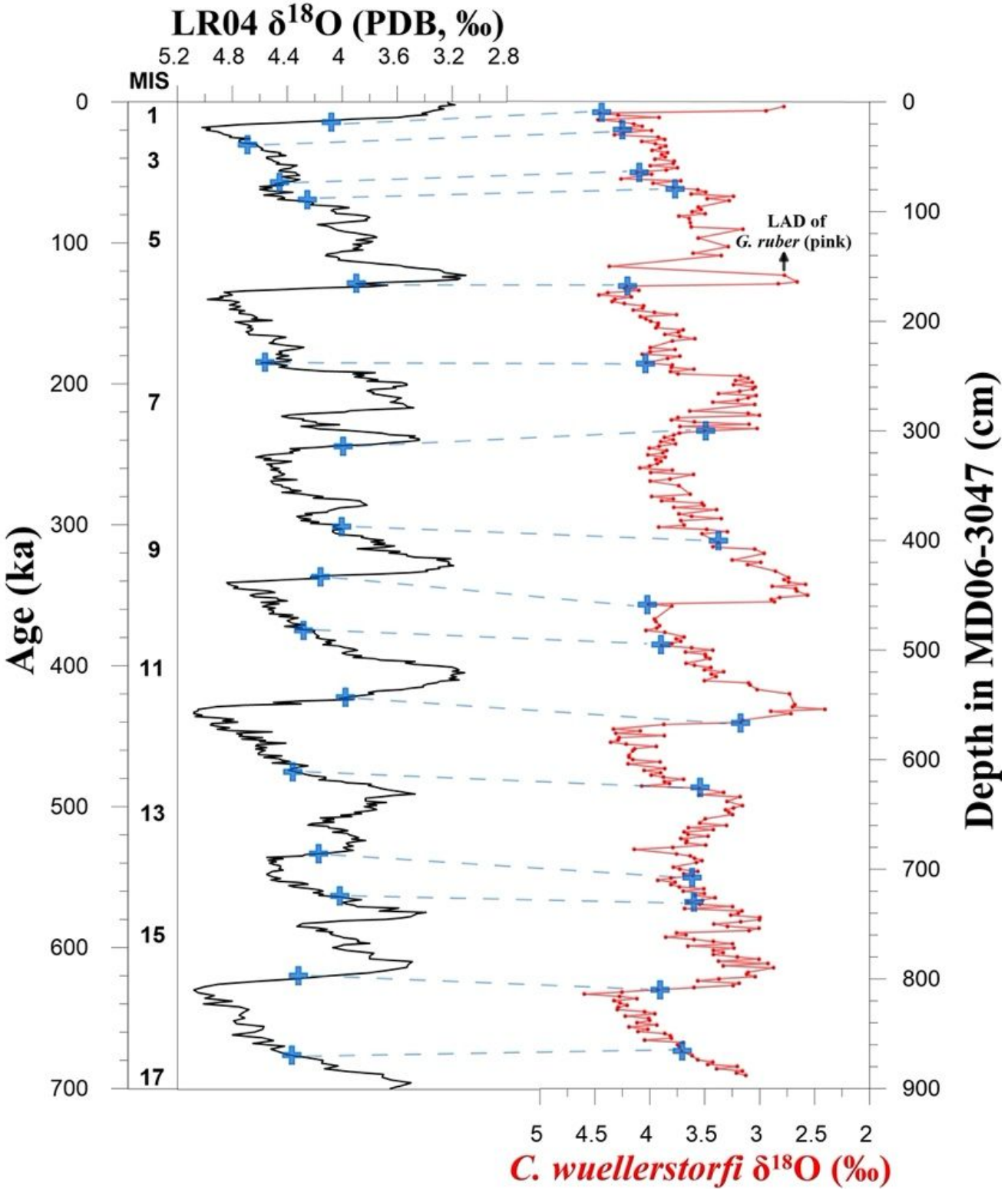

Figure 2

Chronological framework for core MD06-304730, obtained by graphical comparison between the δ18O record of epibenthic foraminifera C. wuellerstorfi and the stacked global benthic LR04 δ18O record31, with additional refinement based on the last appearance datum (LAD) of Globigerinoides ruber (pink). Blue crosses represent oxygen-isotope events, and the black arrow indicates the LAD of G. ruber (pink).

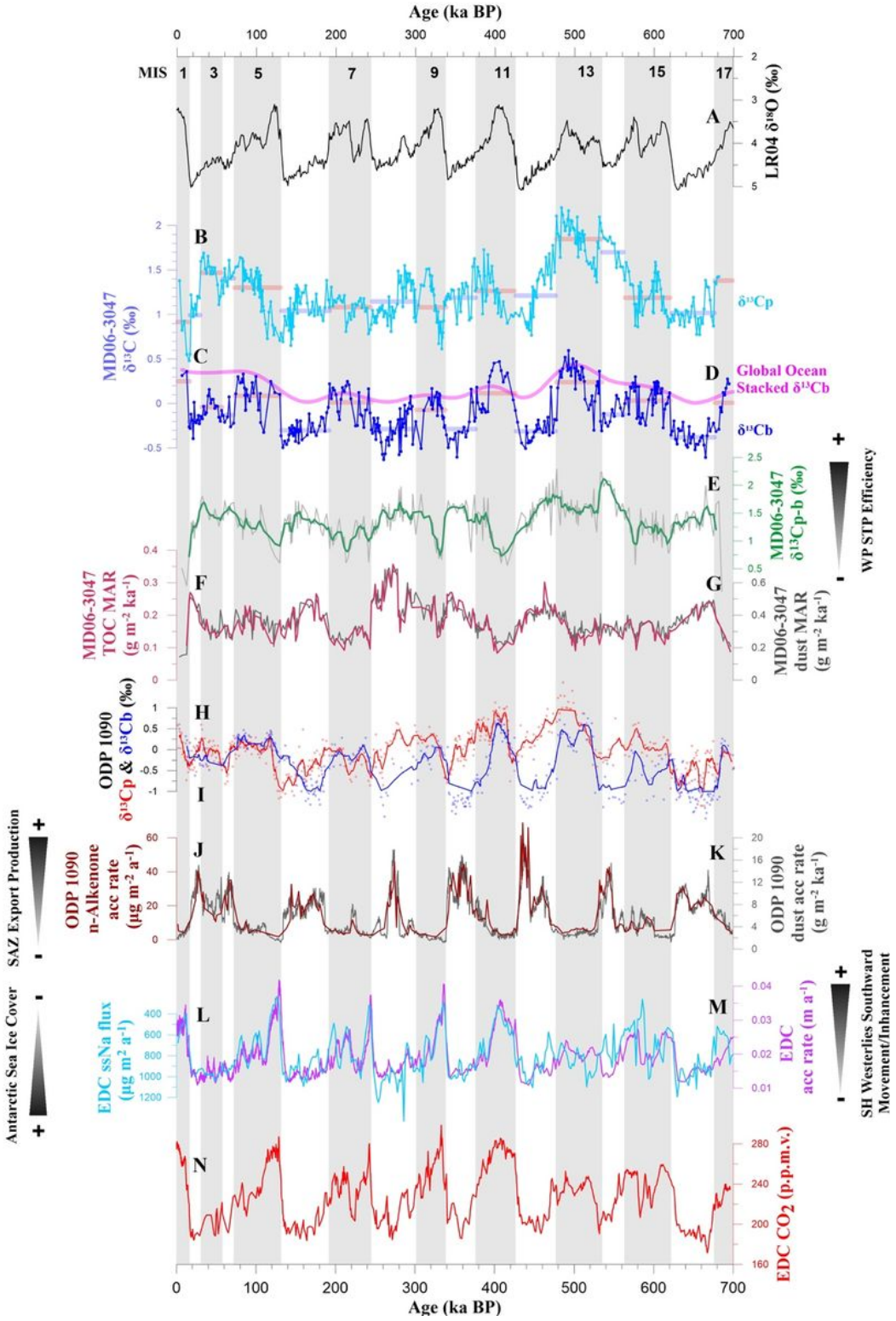

Figure 3

Records of (A) The stacked global benthic LR04 δ18O31, (B) MD06-3047 δ13Cp extracted from thermocline-dwelling planktonic foraminifera (Pulleniatina obliquiloculata), and (C) MD06-3047 δ13Cb extracted from epibenthic foraminifera (Cibicidoides wuellerstorfi). Horizontal red and blue lines in panels B and C represent the average δ13Cp and δ13Cb values of the respective Marine Isotope Stage. (D) Stacked δ13Cb of the global ocean42. (E) MD06-3047 δ13Cp-b; the green line is the five-point running

average. (F) MD06-3047 TOC MAR49. (G) MD06-3047 dust MAR49. (H and I) ODP 1090 δ13Cp and δ13Cb40. (J) Accumulation rate of n-alkenone from ODP 109082. (K) Dust accumulation rate from ODP 109082. (L) Sea-salt sodium (ssNa) flux at EPICA Dome C43(EDC). (M) Accumulation Rate at EDC83. (N) pCO2 record from EDC84. Grey shading indicates interglacial periods.

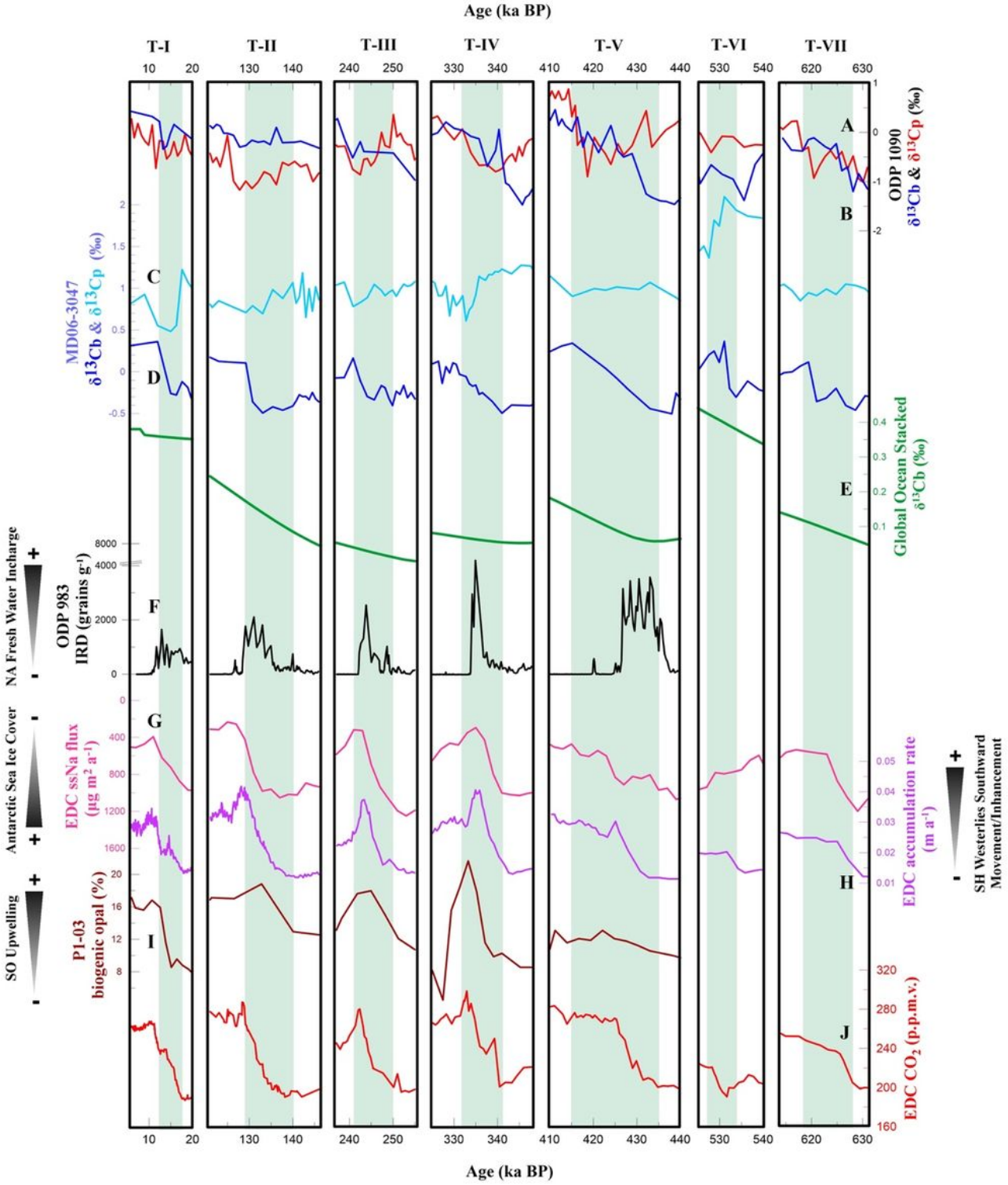

Figure 4

Records of (A and B) δ13Cp and δ13Cb, respectively, from core ODP-109040, as well as (C and D) δ13Cp and δ13Cb, respectively, from core MD06-3047 (this study). (E) Stacked δ13Cb time series for the global ocean42. (F) Ice-rafted debris (IRD) record from ODP 983 in the northeast Atlantic72. (G) ssNa flux at EPICA Dome C43 (EDC). (H) Accumulation Rate at EDC83. (I) Biogenic opal concentration from P1-0369. (J) pCO2 record from EDC84. Green shading indicates glacial terminations.

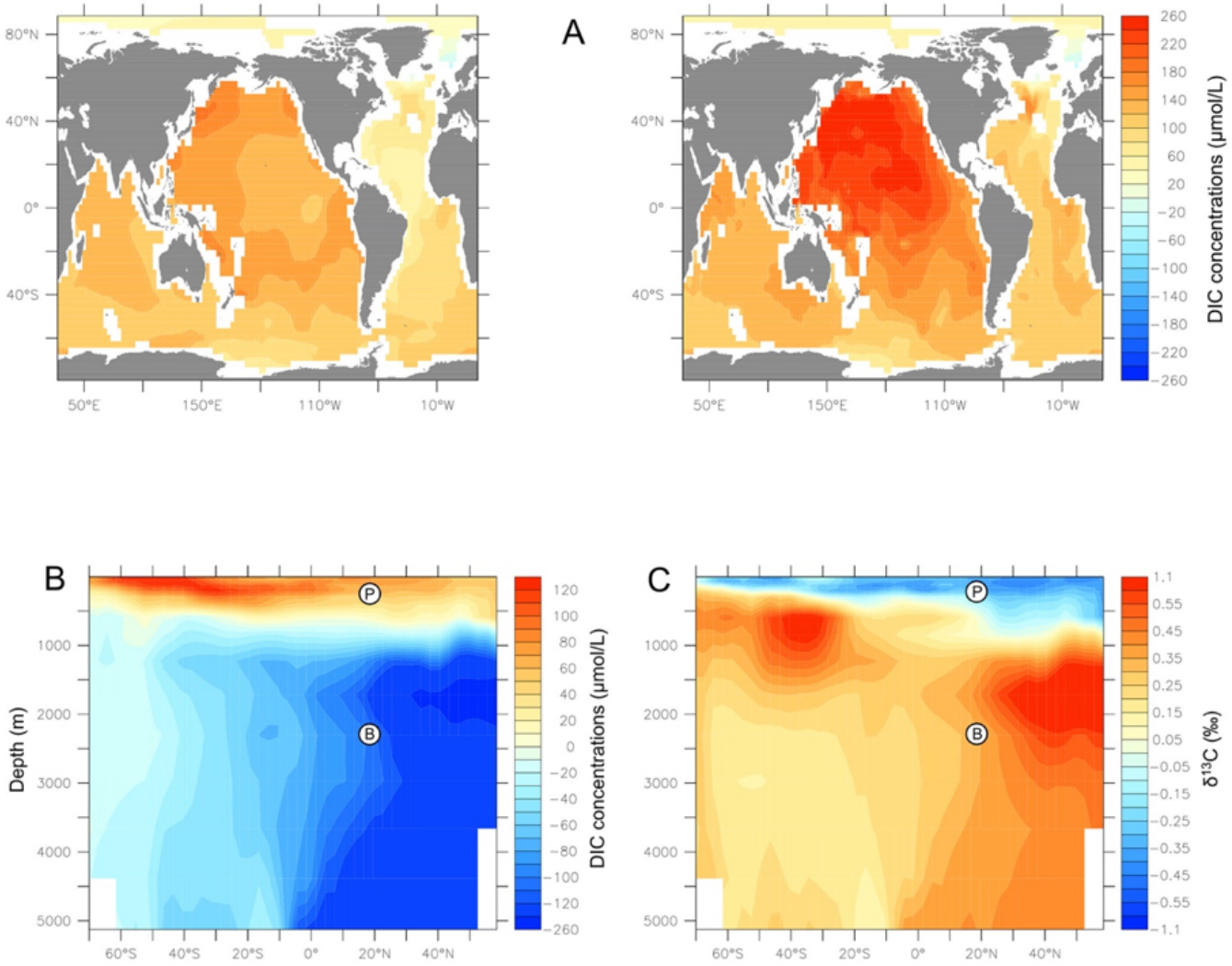

Figure 5

Simulated ocean DIC and δ13C anomalies in model LOVECLIM. Simulated (A) DIC concentration (μmol/L) anomalies at the LGM compared to pre-industrial (PI) at 2500 m depth near the study-core11 (left) and at the bottom (right). (B) DIC concentration (μmol/L) and (C) δ13C (‰) anomalies at HS1 compared with LGM zonally averaged over the Indo-Pacific26. Circle B indicates the position of benthic foraminifera C. wuellerstorfi in core MD06-3047 (17°00.44'N, 124°47.93'E, 2,510 m water depth) and circle P indicates where the subsurface-dwelling planktonic foraminifera P. obliquiloculata records middle to upper thermocline properties.

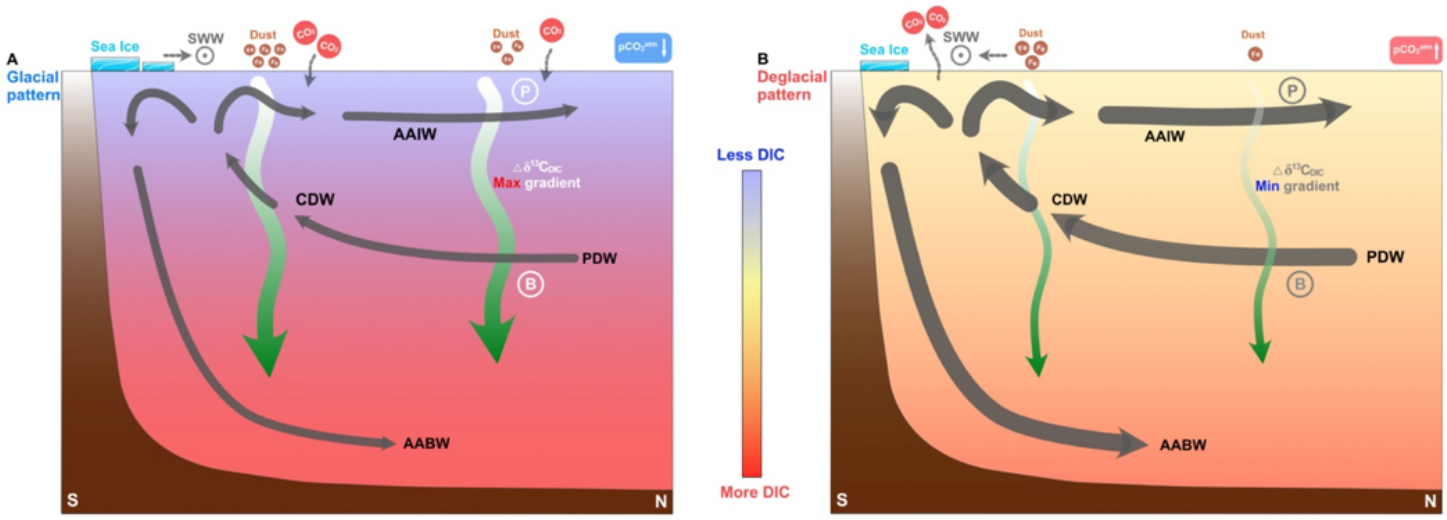

Figure 6

Schematic representation of the South and tropical Pacific overturning circulation. (A) Glacial pattern with more dust input, efficient biological nutrient export, a northernmost extent of sea ice and SWW, a stratified Southern Ocean, DIC sequestration in deep, decreased atmospheric CO2, and a large Δδ13CDIC. (B) Deglacial pattern with upwelling induced by southward shift of Antarctic sea ice and SWW, less dust input, inefficient biological nutrient export, outgassing of CO2, DIC transmission from deep to upper layer, and a consequently small Δδ13CDIC. Grey arrows: overturning circuit; green arrows: biological nutrient export to the ocean interior; light-blue rectangles: sea ice; SWW: Southern Westerly Winds; major water masses (SAMW, AAIW, AABW, CDW, and PDW). Circle B: the position of benthic foraminifera C. wuellerstorfi in core MD06-3047 (17°00.44'N, 124°47.93'E, 2,510 m water depth); and circle P: where the subsurface-dwelling planktonic foraminifera P. obliquiloculata records middle to upper thermocline properties. The thickness of the arrow represents its strength. The color shading of the ocean section represents the DIC concentrations.

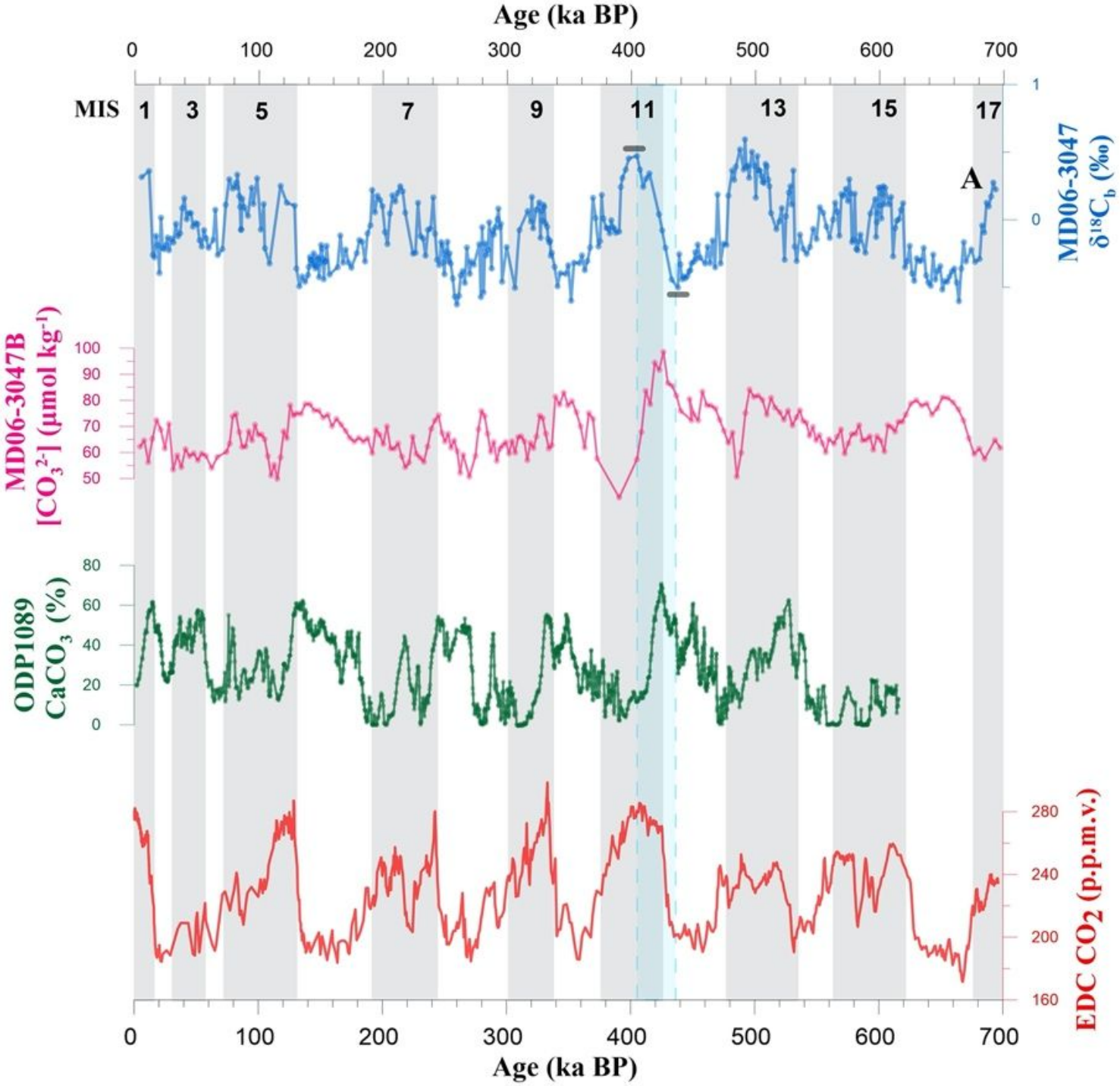

Figure 7

Records of (A) δ13Cb from MD06-3047 (this study) and (B) Deep-water [CO32-] from MD06-3047B78 (same location). (C) Pacific-pattern of deep-sea sedimentary calcium carbonate content change at site ODP 108979 (note that although ODP1089 is from a site in the South Atlantic, it is bathed in Indo-Pacific deep water, rather than North Atlantic Deep Water). (D) pCO2 record from EDC84. Grey shading indicates interglacial periods, light blue shading indicates the MIS12/11 transition.